



# A case study on time-dependent bedding plane failure

Michinori Asaka · Rune Martin Holt

Received: 20 April 2021 / Accepted: 3 December 2022  
© The Author(s) 2023

**Abstract** Time-delayed wellbore failures are often observed in shale formation. In some cases, cavings indicating bedding plane failure are observed a few days after initial drill-out with a gradual increase, eventually leading to wellbore collapse. Possible causes of time-delayed wellbore failure include pore pressure diffusion, and its impact can be assessed by traditional poroelastic modeling in which coupled hydraulic-mechanical processes are taken into account. Externally applied loads induce pore pressure that is dissipated according to a diffusion law. During recently conducted wellbore stability analysis targeting a particular field within a strike-slip regime, we found: (1) time-dependent bedding plane failures are significant for highly inclined wells subparallel to the maximum horizontal stress direction (bedding plane failure region gradually increases with time), (2) the Kirsch solution and the assumption of no induced pore pressure (elastic nonporous model) does not give proper mud weight limits to avoid bedding plane failures, and (3) failure regions and modes predicted by the poroelastic model are different from those based on the elastic nonporous approach, under

the given situation. Results given by the poroelastic model are apparently consistent with filed observations, demonstrating pore pressure diffusion as a possible cause of observed time-delayed bedding plane failure.

## Article Highlights

- Induced pore pressure and its dissipation can lead to significant time-delayed bedding plane failures
- Wellbore failures given by the poroelastic model can be completely different from the elastic nonporous model frequently used in the oil and gas industry
- Results given by the poroelastic model are apparently consistent with field observations

**Keywords** Wellbore stability · Shale · Poroelasticity · Bedding plane failure · Mud weight

## 1 Introduction

Wellbore stability analysis is one of the important elements in drilling operations. Drilling parameters such as mud weight and wellbore orientation (hole inclination and azimuth) have to be correctly optimized to avoid borehole instability. In particular, shale formations are the main source of borehole instability and

---

M. Asaka (✉) · R. M. Holt  
Norwegian University of Science and Technology  
(NTNU), 7491 Trondheim, Norway  
e-mail: michinori.asaka@inpx.co.jp

M. Asaka  
INPEX Corporation, Akasaka Biz Tower 5-3-1, Akasaka,  
Minato-ku, Tokyo 107-6332, Japan

a good understanding of the mechanical behavior of shales is required. Borehole collapse criteria are traditionally given based on linear elasticity theory combined with brittle failure mechanics, however, a more sophisticated approach is required to tackle complex problems such as time-delayed wellbore failures.

Time-delayed wellbore failures are often observed in shale formation. In some cases, cavings indicating bedding plane failure are observed few days after initial drill-out with a gradual increase, eventually leading to wellbore collapse. However, there are few publications where time dependence is modelled specifically for a given case. This is particularly the case for bedding plane failures, as addressed here. Possible causes of the time-delayed wellbore failure include (1) Pore pressure diffusion, (2) Cooling of formation by drilling fluid, (3) Chemical interaction between drilling fluid and shale formation, and (4) Creep. The impact of pore pressure diffusion can be investigated by the theory of poroelasticity. It was first introduced by Biot (1941) and has been revisited from various points of view. For example, Rice and Cleary (1976) reformulated the Biot theory in terms of parameters which are more open to physical interpretation. Detournay and Cheng (1988) provided analytical solutions for poroelastic response of a borehole based on the reformulation. Coupled hydraulic-mechanical processes are taken into account by the poroelastic model; externally applied loads induce pore pressure which is dissipated according to a diffusion law. Both drained and undrained rock moduli and Skempton's  $B$  parameter are required for the poroelastic models. Measuring these parameters is possible (Holt et al. 2018a,b), though it is time consuming, challenging and non-standard for most laboratories. Extension of this theory to incorporate material anisotropy has been addressed by several authors. Available analytical solutions for transversely isotropic materials (e.g., Abousleiman and Cui 1998) assume that the plane of isotropy always is perpendicular to the borehole axis. Numerical modeling is required to remove this assumption (Kanfar et al. 2015).

Thermoporoelastic models (e.g. Abousleiman and Ekbote 2005; Gao et al. 2017a,b; Ghassemi and Diek 2002) provide the coupled thermo-hydraulic-mechanical behavior of fluid saturated rock, but additional input parameters are required. Additional parameters include linear expansion coefficient for solid matrix, volumetric expansion coefficient for fluid, thermal

diffusivity and thermo-osmotic coefficient. Uncertainty in these parameters and assumptions could have significant impact on the result. For example, pore pressure can either be increased or decreased when cooling wellbore, depending on the magnitude and sign of the thermo-osmotic coefficient (Ghassemi and Diek 2002). Chemical mechanisms that may lead to interaction between shale and drilling fluid includes osmosis (Fjaer et al. 2008). Mody and Hale (1993) implemented osmotic theory into a rock mechanics model for borehole stability by adding the osmotic potential through a stress term. Ionic exchange may also occur within the shale when it is exposed to brine. In particular, exposure of smectite-rich shale to KCl causes significant shrinkage (Horsrud et al. 1998). Creep is related to deformation at the atomic / molecular scale, in which the material keeps deforming without any increase in the applied stress (Fossen 2016). The strain–time curve for a creeping material can be characterized by three stages of creep. The first stage of creep is called transient creep; the second stage is called steady-state creep; the third stage is called accelerating creep where microfracturing causes an increase in strain rate which leads rapidly to failure (Fossen 2016; Fjaer et al. 2008).

In this paper, time-delayed wellbore failures (in particular time-delayed bedding plane failure) caused by pore pressure diffusion were investigated targeting a particular field within a strike-slip regime. Time-delayed bedding plane failure has been addressed by e.g. Kanfar et al. (2015), who investigated the impact of elastic anisotropy, while Ma et al., (2018) showed an example where the changes in the strength of weak plane with exposure to mud is the predominant source of the failure zones enlargement. Here, we will demonstrate that the pore pressure diffusion can cause significant time-delayed bedding plane failures. Detailed investigations were performed including changes in stress acting on bedding plane and safe mud weight limits as time progresses. Stress concentration and induced pore pressure around an inclined circular borehole is calculated based on the traditional isotropic poroelastic model of Detournay and Cheng (1988). The model is easy to implement and input parameters can be reasonably estimated as demonstrated here, hence it is convenient for practical implementation. To account for weak bedding planes, two Mohr–Coulomb failure criteria are adopted, one for the intact rock and the other for the weak bedding

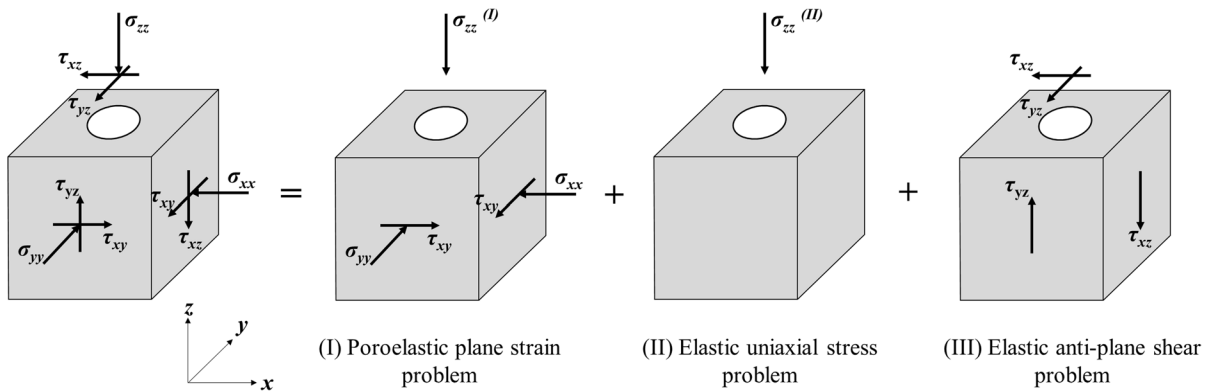


**Fig. 1** Decomposition of the poroelastic borehole problem

plane. Key observations include: (1) time-dependent bedding plane failures are significant for highly inclined wells drilled subparallel to the maximum horizontal stress direction (bedding plane failure region gradually increase with time), (2) the Kirsch solution and the assumption of no induced pore pressure (i.e., elastic nonporous approach) does not give proper mud weight limits to avoid bedding plane failures, and (3) failure regions and modes predicted by the poroelastic model are different from those based on the elastic nonporous approach, under the given situation. Results given by the poroelastic model are apparently consistent with filed observations, demonstrating pore pressure diffusion as a possible cause of observed time-delayed bedding plane failure.

## 2 Method

### 2.1 Poroelasticity and analytical solutions

Detournay and Cheng (1988), based on the Biot theory and Darcy’s law, provided analytical solutions in the Laplace transform space for stress concentration and induced pore pressure around a circular borehole. In this paper, wellbore stability analyses is performed based on the analytical solutions. A set of bulk material constants is required as an input: fluid viscosity  $\mu$ , permeability  $k$ , rock shear modulus  $G$ , drained/undrained rock Poisson’s ratio ( $\nu$  and  $\nu_u$ ) and Skempton’s  $B$ . All these constants can be measured experimentally (e.g. Holt et al. 2018a, b). The generalized consolidation coefficient  $c$ , which characterizes the diffusion process, is calculated as follows:

$$c = \frac{2B^2 G_\mu^k (1 - \nu)(1 + \nu_u)^2}{9(1 - \nu_u)(\nu_u - \nu)} \tag{1}$$

The borehole drilling is simulated by removing the stresses acting on the borehole wall and setting the well pressure to a specified value  $q$ . According to the loading decomposition scheme proposed by Abou-Isleiman and Cui (1998), the poroelastic problem can be decomposed into three sub-problems to simplify the analysis (see also Gao et al. 2017a, b); (I) a poroelastic plane strain problem, (II) an elastic uniaxial stress problem, and (III) an elastic anti-plane shear problem (Fig. 1). The poroelastic plane strain problem (sub-problem I) is concerned with diffusion and poroelastic processes caused by the presence of borehole in a saturated formation subject to in-situ stress under the assumption of plane strain conditions. The solution of the elastic uniaxial stress problem (sub-problem II) gives a constant vertical stress everywhere which accounts for the far-field in situ stresses and virgin pore pressure. The elastic anti-plane shear problem (sub-problem III) is related to the shear deformation which is uncoupled with the pore fluid flow because of no volumetric strain. The poroelastic plane strain problem (sub-problem I) can further be decomposed into three fundamental modes; (1) differential pressure between the far-field isotropic stress and well pressure (Mode 1), (2) differential pressure between virgin pore pressure and well pressure (Mode 2), and (3) a far-field deviatoric stress (Mode 3). Mode 1 and 2 are axisymmetric, which give a homogeneous diffusion equation, while mode 3 is asymmetric. Mode 1 is purely elastic. The principle of

superposition is then used to obtain the complete solutions. Note that the traditional top-of-hole borehole coordinate system where  $x$ -axis points to the upward direction in the cross-sectional plane was used in this study. In-situ stresses are therefore transformed to the coordinate system by conducting two rotations to obtain the far field in situ stress components ( $\sigma_{x,0}$ ,  $\sigma_{y,0}$ ,  $\sigma_{z,0}$ ,  $\tau_{yz,0}$ ,  $\tau_{xz,0}$  and  $\tau_{xy,0}$ ): first to the global coordinate system; second to the traditional top-of-hole borehole coordinate system according to the well azimuth and inclination. Analytical solutions require the following parameters related to the far field stress components:

$$\begin{aligned}\sigma_m &= \frac{\sigma_{x,0} + \sigma_{y,0}}{2} \\ \sigma_d &= \frac{\sqrt{(\sigma_{x,0} - \sigma_{y,0})^2 + 4\tau_{xy,0}^2}}{2} \\ \theta_r &= \frac{1}{2} \tan^{-1} \frac{2\tau_{xy,0}}{\sigma_{x,0} - \sigma_{y,0}}\end{aligned}\quad (2)$$

Solutions for each problem are given in Appendix A (see Detournay and Cheng 1988; Abousleiman and Cui 1998 for their derivations; see also Cui et al. (1997a, 1999) for essentially the same approach). Here, positive stress denotes compression although the solutions were originally obtained on the condition that tension is positive.

The applicability of Biot's theory of poroelasticity and Darcy's law to clays and shales has been investigated by several authors. Berti and Simoni (2010) analyzed the hydrologic response of an unstable clay slope to rainfall, and found that the short-term behavior can be reasonably reproduced by the 1D linear diffusion model proposed by Iverson (2000). Hachem (2017) examined existing (Brewster 2015) and new consolidation/pulse tests on fire clay, and demonstrated that measured pore pressure responses and deformations can be well explained by the analytical model based on the theory of poroelasticity and Darcy's law. Pore pressure responses shown in Hachem (2017) clearly show the coupled hydraulic-mechanical processes; externally applied stresses increase pore pressure which is then decreased due to the expulsion of the fluid. Holt et al. (2018a) showed that static behavior of shale in terms of undrained vs drained moduli, Skempton's parameters

and Biot coefficients is reasonably described by the poroelasticity theory.

## 2.2 Failure criteria

Shales usually contain weak planes such as beddings, and both compressive strength and failure mode vary as a function of the loading angle. Two Mohr–Coulomb failure criteria are therefore adopted; shear failure across the intact rock and the slippage along the weak bedding planes as demonstrated by Lee et al. (2012). The Mohr–Coulomb failure criterion for the intact rock is expressed as (Fjaer et al. 2008):

$$\sigma'_1 = C_0 + \sigma'_3 \tan^2 \beta \quad (3)$$

where  $\sigma'_1$  and  $\sigma'_3$  are the maximum and minimum effective principal stresses, respectively.  $C_0$  is the uniaxial compressive strength and  $\beta = \pi/4 + \varphi_f/2$  ( $\varphi_f$  is the friction angle). Jaeger and Cook (1979) gave the following formula for the Mohr–Coulomb failure criterion for the weak bedding planes:

$$\tau_w = S_w + \mu_w \sigma'_w \quad (4)$$

where  $\tau_w$  and  $\sigma'_w$  are the shear and effective normal stresses acting on the plane of weakness (bedding), respectively.  $S_w$  and  $\mu_w$  are the cohesion and the sliding friction coefficient of the plane of weakness, respectively. Note that the stresses have to be projected onto the surface of bedding plane by stress transformation to obtain the shear and effective normal stresses.

Tensile failure was also considered, which takes place when the effective tensile stress at the borehole wall is equal to the tensile strength  $T$  of the rock. Note that the Terzaghi effective stress was used for failure predictions since it is generally accepted that compressive failure, as well as tensile failure, is controlled by the Terzaghi effective stress (Cornet and Fairhurst 1974; Fjaer et al. 2008; Bouteca and Gueguen 1999).

## 3 Wellbore stability analysis

### 3.1 Observations

The wellbore failure prediction was conducted targeting a particular field. The field is located within the Browse Basin on the North West Shelf of Australia,

which is considered to be one of the most prolific areas in terms of hydrocarbon accumulation in Australia. Several time-delayed bedding plane failures have been observed and one of them is described here.

The 12.25-inch section of the well A was drilled through the deeper part of a thick shale section at 70° hole inclination in a direction subparallel to the maximum horizontal stress. While circulating and conditioning the hole, high torque and pack-off events occurred. Back-reaming out of the hole for about 8 h appeared to be successful, although large volumes of cuttings and tight hole conditions were observed. Mud-weight was increased, followed by multiple string stalls, high torque, and blocky cavings in the shakers. An extensive conditioning and cleaning of the hole were attempted, but lead to the drill string becoming stuck and plugged after observing little to no returns. Pulling-out-of-hole (POOH) without pumping was the only option because circulation could not be regained. The 12.25-inch hole section had no issues when originally drilling through the middle of the thick shale section about 5 days earlier. However, while dry-reaming out of the hole, numerous tight hole, stuck pipe, and high torque events occurred. These troubles eventually caused impasse situations. An extensive effort to free the drill string managed to resume POOH, however, the drill bit and a section of the power-drive were left in the hole. The decision was made to run-in-hole with a clean-out bottom-hole-assembly.

Cleaning out the well proved to be problematic. Multiple tight spots associated with the mechanical drill string problems (e.g., high torque, overpull etc.) were observed in the middle of the thick shale section. These problems were followed by large volumes of drilling cuttings and blocky cavings in the shakers when circulation was re-established. The blocky cavings seemed to have originated in the thick shale section. Reaming in hole and back-reaming operations failed to clean out the well any deeper than the middle of the thick shale section. The decision was made to POOH while back-reaming in preparation for a sidetrack.

The blocky and planar geometry of the observed cavings suggested that time-delayed bedding plane failures were the main cause of wellbore instabilities.

**Table 1** Input parameters for the wellbore stability analysis. Stresses and pore pressure are given in  $\text{g/cm}^3$  to facilitate the comparison with the mud weight

Well depth (m)	3100
Wellbore azimuth (drilling direction)	N70°E
Wellbore inclination (deg.)	70
Overburden stress ( $\text{g/cm}^3$ )	2.0
Maximum horizontal stress ( $\text{g/cm}^3$ )	2.39
Minimum horizontal stress ( $\text{g/cm}^3$ )	1.77
Maximum horizontal direction	N90°E
Virgin pore pressure ( $\text{g/cm}^3$ )	1.5
Mud weight ( $\text{g/cm}^3$ )	1.63
UCS of rock matrix (MPa)	55
Coefficient of friction of rock matrix	0.6
Tensile strength of rock matrix (MPa)	0
Porosity	0.2
Permeability ( $\text{m}^2$ )	$10^{-21}$
Density ( $\text{g/cm}^3$ )	2.42
Undrained vertical P-wave velocity (km/s)	2.41
Undrained vertical S-wave velocity (km/s)	1.1
Undrained Young's modulus (GPa)	8.01
Shear modulus of rock (GPa)	2.93
Undrained Poisson's ratio	0.37
Grain bulk modulus (GPa)	25
Fluid bulk modulus (GPa)	2.6
Fluid viscosity ( $\text{Pa}\cdot\text{s}$ )	$10^{-3}$
Calculated Skempton $B$	0.85
Calculated Biot coefficient	0.91
Cohesion of weak plane (MPa)	2
Coefficient of sliding friction of weak plane	0.5
Dip angle of weak plane (deg.)	0

### 3.2 Input parameters

The input parameters for the wellbore stability analysis are listed in Table 1. As shown in the table, in situ stress state is a strike-slip regime with significant stress anisotropy (note that the maximum and minimum horizontal stresses correspond to approximately 73 and 54 MPa, respectively) (Asaka et al. 2016). The target interval is the aforementioned thick shale interval, corresponding to Cretaceous age. It mainly consists of claystone or calcareous claystone, and depositional environment is interpreted as distal shelf. Drilling direction and hole inclination is the same as the well A mentioned in the previous section (i.e., a

highly inclined well subparallel to the maximum horizontal stress direction). Drilling fluid was synthetic oil which generally prevents fluid pressure invasion into the formation (i.e., impermeable boundary condition); induced pore pressure and stresses associated with the mode 2 is therefore set to zero in this case (e.g., Roohi 2017). Permeability is assumed to be 1 nD, which is within general range of reported shale permeabilities (MacBeth et al. 2011). Elastic properties of undrained shale are based on log data. The lack of input data limits the elastic and permeability descriptions to be isotropic although the problem addressed is linked to anisotropy in strength which was taken into account by including the weak plane. Moreover, sonic log data provide dynamic elastic moduli, which represent upper limits to undrained static stiffnesses. Plasticity is also important for quantitative prediction of critical mud weight. However, due to the lack of data, conversion of dynamic moduli to static moduli and plasticity were not accounted for in the current analysis; our focus here is to identify possible cause of time-delayed bedding plane failure rather than precise prediction of critical mud weight. Unconfined compressive strength (UCS) is based on the rock mechanics test conducted for shale rocks at slightly deeper depth level. Skempton  $B$  and drained rock properties have not been measured in this field, and they therefore need to be estimated. Those bulk material constants can be estimated from a set of basic material parameters such as grain and fluid bulk modulus and porosity as follows (Fjaer et al. 2008):

$$B = \frac{\frac{K_f}{\Phi} \left(1 - \frac{K}{K_s}\right)}{\frac{K_f}{\Phi} \left(1 - \frac{K}{K_s}\right) + K \left(1 - \frac{K_f}{K_s}\right)} \quad (5)$$

where  $\Phi$  is porosity,  $K_f$  is fluid bulk modulus, and  $K_s$  is grain bulk modulus. Drained rock bulk modulus  $K$  can be calculated by inverse Gassmann's equation (e.g. Smith et al. 2003):

$$K = \frac{K_u \left( \frac{\Phi K_s}{K_f} + 1 - \Phi \right) - K_s}{\frac{\Phi K_s}{K_f} + \frac{K_u}{K_s} - 1 - \Phi} \quad (6)$$

where  $K_u$  is undrained rock bulk modulus. Fluid bulk modulus was estimated from known temperature, pressure and salinity using Batzle and Wang equations (Batzle and Wang 1992). Grain bulk modulus is assumed to be isotropic with a value of 25 GPa. This

value is based on clay velocity interpreted by extrapolating empirical relations (Castagna et al. 1993) and similar to the estimated value based on anisotropic poroelasticity by Holt et al. (2018a). The calculated Skempton  $B$  is 0.85. Actual input mud weight is used in the existing inclined well. It was determined by the elastic nonporous wellbore stability analysis based on the Kirsch solution without consideration of time-dependent wellbore failure. Cohesion and sliding friction coefficient for weak plane were previously determined so that the elastic nonporous wellbore stability analysis using those parameters can reasonably explain the observed drilling events in some of existing wells. Seismic depth structures suggest that dip angle of weak plane (bedding plane) is almost 0 degree (e.g., horizontal bedding plane).

### 3.3 Stress concentration and induced pore pressure

Figure 2 shows induced pore pressure (changes from the virgin pore pressure) variations with radius at sides and top/bottom of borehole. Induced pore pressure variations are shown at 1 h, 1 day, 7 days, and 30 days after drill-out. Instantaneous response was also calculated from stress concentration based on the Kirsch solution (Bradley 1979; Kirsch 1898; Hiramoto and Oka 1962) and Skempton  $B$ . Induced pore pressure (Mode 3 only in this case) largely depends on stress concentration. Large tangential and axial stresses at sides of borehole (Fig. 3) results in large positive induced pore pressure while top and bottom of borehole shows large negative induced pore pressure at early times. Those induced pore pressures are dissipated at longer times. The magnitude of the induced pore pressure can be ~5 MPa in this case, which cannot be ignored in practice. Figure 3 shows corresponding stress concentration variations with radius. Tangential and axial stresses show relatively large time-lapse changes.

Figure 4 shows comparisons of induced pore pressure and stress concentration variations with angular borehole position at 7 days after drill-out with the instantaneous responses based on the Kirsch solution at radius ratio ( $r/a$ ) of 1.04. As demonstrated in Fig. 2, top/bottom of borehole show instantaneous negative induced pore pressure, while sides of borehole show instantaneous positive induced pore pressure. These induced pore

**Fig. 2** Induced pore pressure (changes from the virgin pore pressure) variation with radius at top/bottom of borehole (left) and sides of borehole (right) for a highly inclined well subparallel to the maximum horizontal stress direction

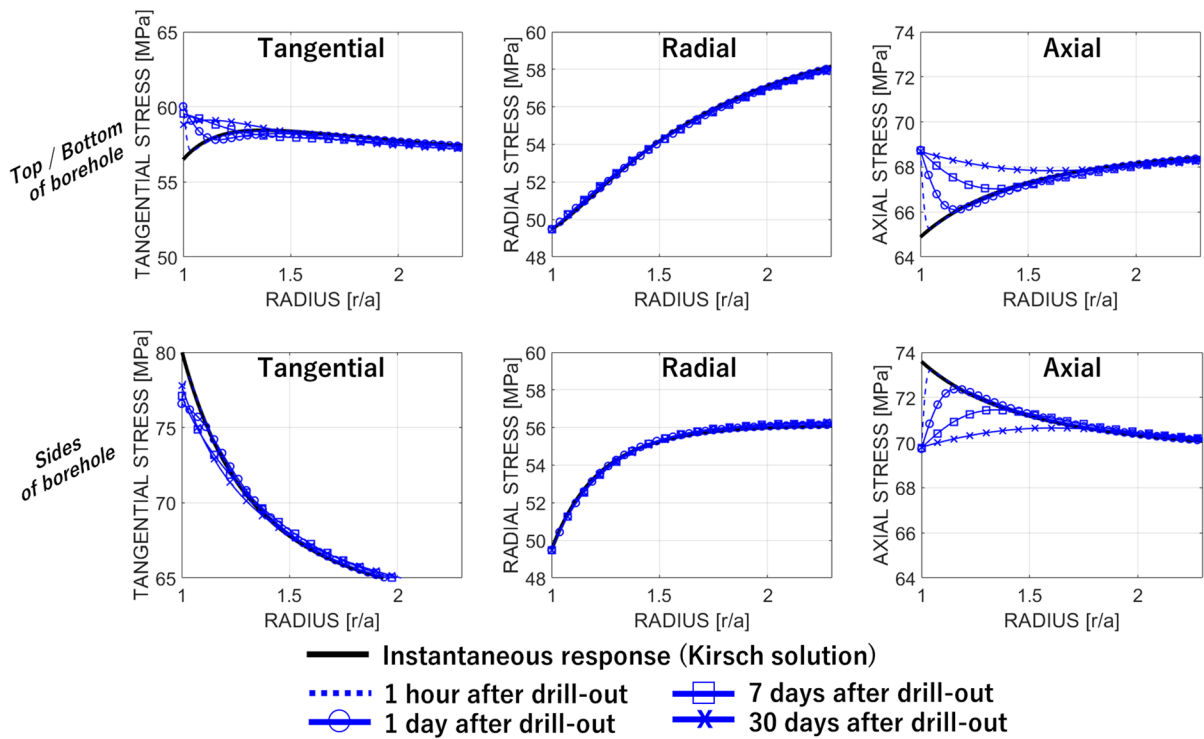
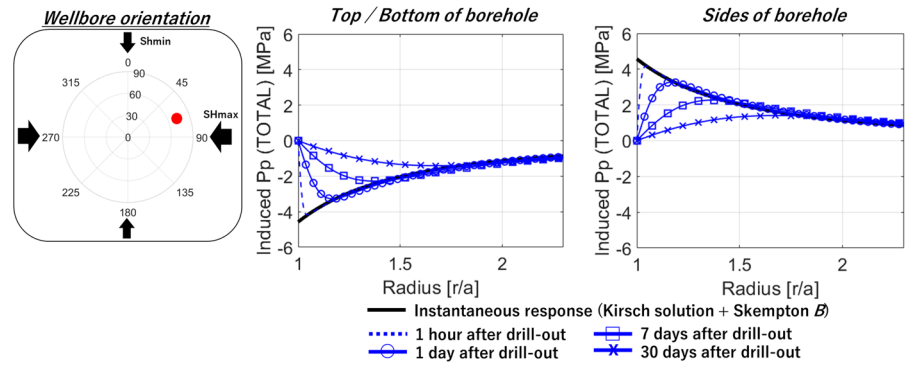


**Fig. 3** Stress concentration variation with radius at top/bottom of borehole (top) and sides of borehole (bottom) for a highly inclined well subparallel to the maximum horizontal stress direction

pressures are however almost dissipated at 7 days after drill-out. These pore pressure and stress changes could have significant impact on the borehole failure prediction because of changes in effective stress. To see the impact, principal effective stresses and shear and normal effective stresses acting on the bedding plane at 7 days after drill-out were compared with the instantaneous responses.

Note that bedding plane is horizontal and stress transformation was performed to obtain the shear and effective normal stresses, as mentioned earlier. Figure 5 shows the comparison. As shown in the figure, minimum principal effective stress is decreased at borehole positions with instantaneous pore pressure reduction. This may trigger shear failures across the intact rock depending on rock

**Fig. 4** Comparisons of induced pore pressure (changes from the virgin pore pressure) and stress concentration at 7 days after drill-out with the instantaneous responses based on the Kirsch solution at radius ratio ( $r/a$ ) of 1.04 for a highly inclined well subparallel to the maximum horizontal stress direction

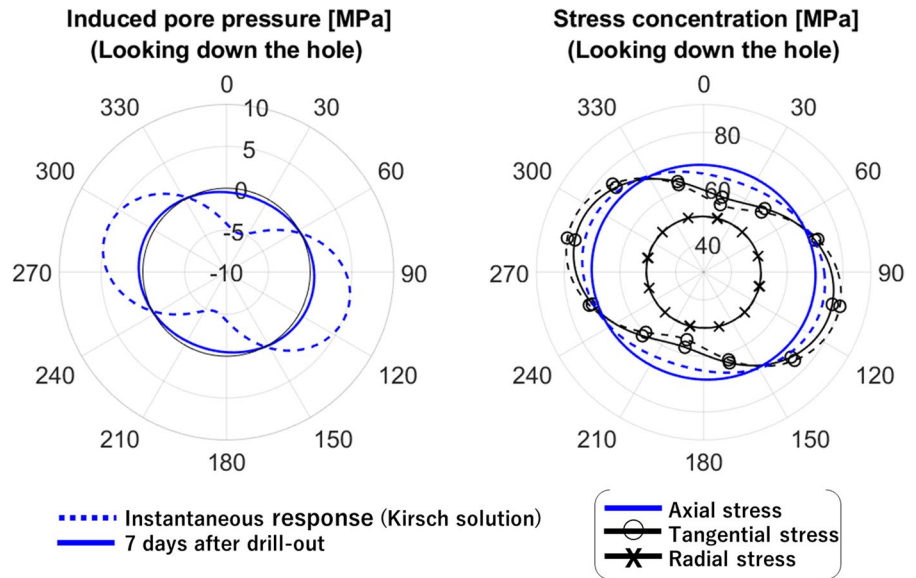
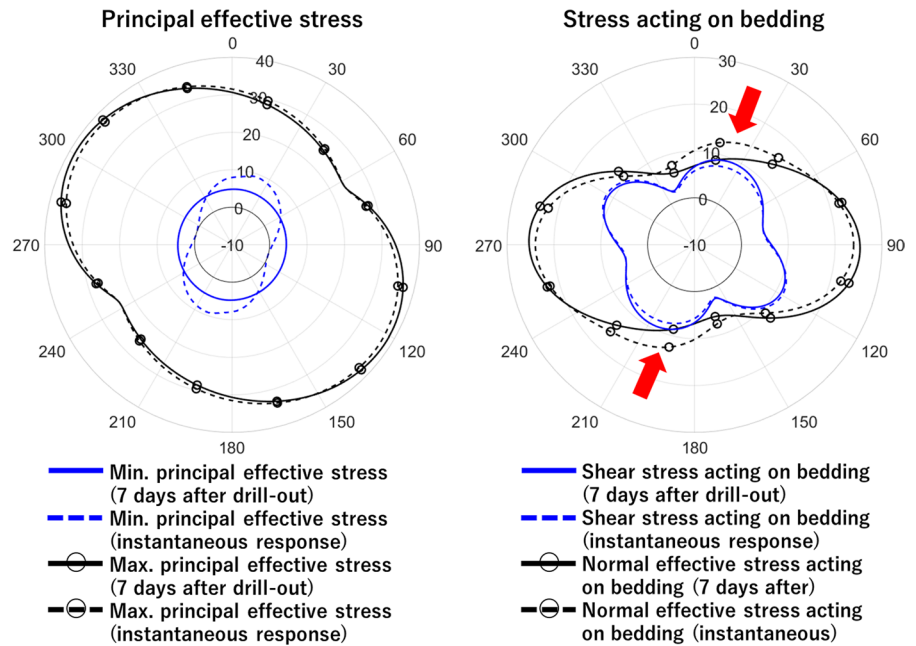


**Fig. 5** Comparisons of principal effective stresses (left) and stresses acting on the bedding plane (right) at 7 days after drill-out with the instantaneous responses at radius ratio ( $r/a$ ) of 1.04 for a highly inclined well subparallel to the maximum horizontal stress direction

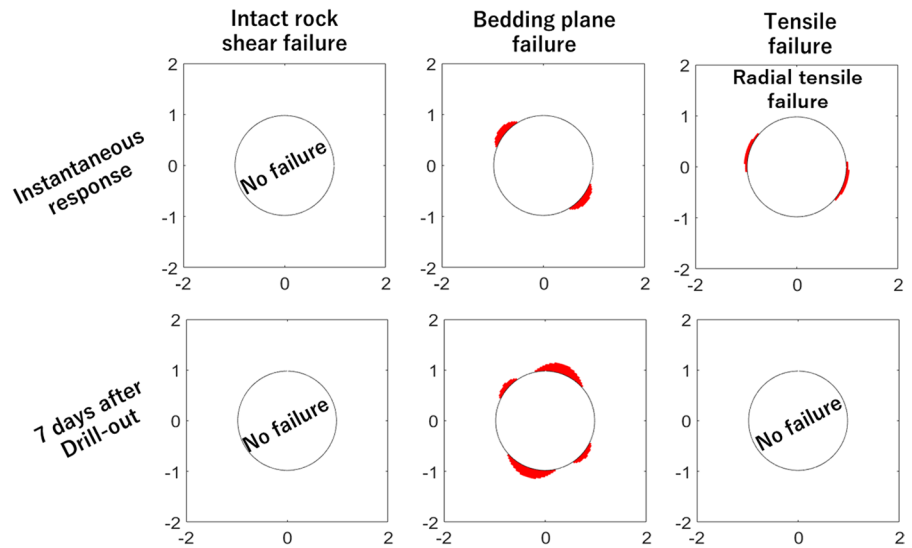


strength. Moreover, the reduction of normal effective stress acting on bedding plane is noticeable at the positions (red arrows in Fig. 5); it becomes smaller than shear stress acting on bedding at 7 days after drill-out. This is because of pore pressure increase and may trigger time-delayed bedding plane failures.

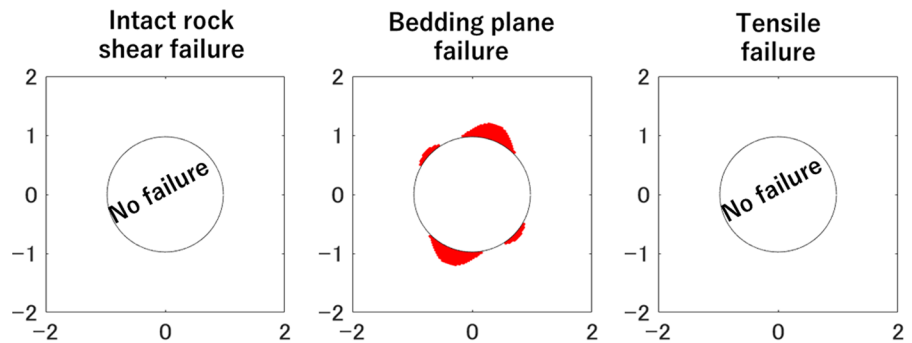
### 3.4 Failure region prediction

Figure 6 shows a comparison of predicted failure regions based on stress state at 7 days after drill-out with that based on the instantaneous response. Three different failure regions were predicted; (1) shear failure across the intact rock, (2) slippage

**Fig. 6** A comparison of failure regions based on stress state at 7 days after drill-out (bottom) with that based on the instantaneous response (top) for a highly inclined well subparallel to in the maximum horizontal stress direction



**Fig. 7** Failure regions predicted by the elastic nonporous approach (Kirsch solution + no induced pore pressure)



along the bedding planes, and (3) tensile failure (tensile fracture + radial tensile failure (tensile failures throughout the wellbore circumference (Fjaer et al. 2008; Skea et al. 2018); radial tensile failures were identified when the angle between the minimum principal stress and radial directions is less than 10 degrees). Increased bedding plane failure regions at 7 days after drill-out are observed. As discussed in the previous section, this is because of reduction of normal effective stress acting on bedding plane where it is close to shear stress acting on bedding plane. This is usually the case for highly inclined wells subparallel to the maximum horizontal stress direction. The observation demonstrates pore pressure diffusion as a possible cause of observed time-delayed bedding plane failure. It should also be mentioned that this example shows radial tensile failure at borehole positions with instantaneous pore pressure increase.

#### 4 Discussion

It was demonstrated that pore pressure diffusion can cause time-delayed bedding plane failure. This is largely due to the induced pore pressure. However, the elastic nonporous approach (the Kirsch solution with no induced pore pressure) is still used in the oil and gas industry. A comparison of these two approaches are given here. Figure 7 shows failure regions predicted by the elastic nonporous approach (Kirsch solution + no induced pore pressure) for the wellbore orientation investigated in the previous section. Predicted failure regions are different when predicted from the poroelastic model. The main difference is that the elastic nonporous approach does not give radial tensile failures because of no induced pore pressure. Note also that, although bedding plane failure regions are almost the same, those given by the poroelastic approach is time-delayed. Unexpected

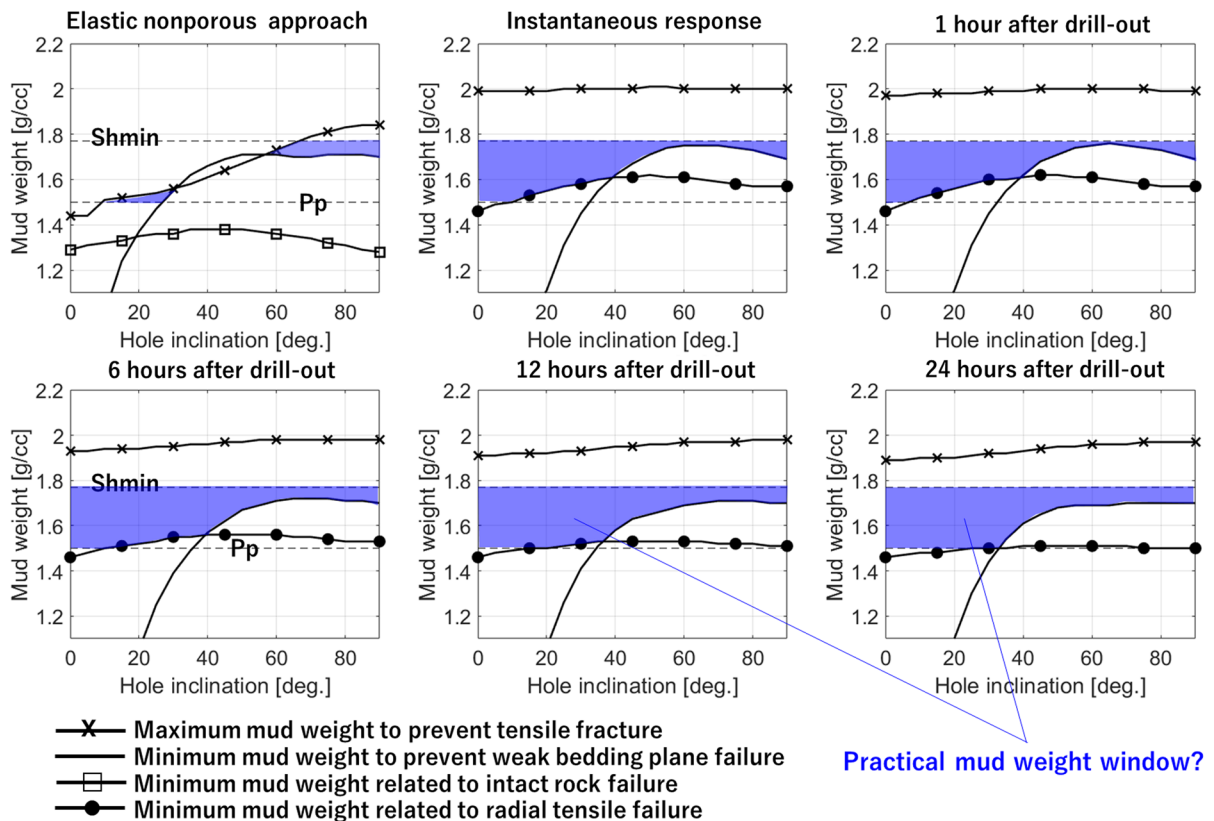


**Fig. 8** A comparison of maximum/minimum mud weights for wells drilled subparallel to the maximum horizontal stress direction (N70°E) based on the elastic nonporous approach, that based on the instantaneous response, and that based on the stress state at 1, 6, 12, 24 h after drill-out. Stress and pore

pressure at radius ratio ( $r/a$ ) of 1.04 was used. Minimum mud weights for intact rock shear failure and radial tensile failure are calculated to prevent specified failure width. The minimum horizontal stress and pore pressure before drill-out are shown as black dashed lines

wellbore failures may therefore happen without consideration of coupled hydraulic-mechanical processes.

The maximum/minimum mud weights required to prevent wellbore failures was also investigated. Figure 8 shows a comparison of the maximum and minimum mud weights for the drilling direction investigated in the previous section based on the elastic nonporous approach (the Kirsch solution + no induced pore pressure), that based on the instantaneous responses (the Kirsch solution + Skempton  $B$ ), and that based on the stress state at 1, 6, 12, 24 h after drill-out. Stress and pore pressure at radius ratio ( $r/a$ ) of 1.04 was used for all calculations since those at the radius ratio of 1 (i.e. at borehole wall) are almost time-independent as shown in Fig. 1 and 2. The same input parameters are used (Table 1). The minimum mud weights related to intact rock shear failure and

radial tensile failure were calculated to prevent specified failure width (90 degrees wide for vertical wells and 30 degrees wide for horizontal wells; those values were linearly interpolated for other inclinations) to show practical mud weight limits. Key findings are as follows:

- The minimum mud weight required to prevent bedding plane failure given by the poroelastic model is initially larger than that based on the elastic nonporous model for highly inclined wells.
- The poroelastic model does not predict shear failures across the intact rock in this case. Instead, radial tensile failures are predicted. This is because induced pore pressure makes the effective radial stress smaller than the tensile strength at angular borehole positions with high hoop stress when low



**Fig. 9** Splintery cavings from breakouts in the thick shale section in the existing vertical well

mud weight is used (tensile strength needs to be higher to have intact rock shear failures). Moreover, the minimum mud weight required to prevent the radial tensile failure is larger than that to prevent the intact shear rock failures predicted by the elastic nonporous approach.

- The maximum mud weight to prevent tensile fractures given by the poroelastic model is substantially larger than that based on the elastic nonporous approach. It decreases gradually as a function of time, but it is still larger than the minimum horizontal stress at 24 h after drill-out (it is still larger at 7 days after drill-out). Note that the maximum mud weight is limited by the minimum in-situ stress to avoid mud losses associated with opening and growth of existing fractures, so that if the limit for tensile fracturing is above this, it is outside of the mud weight limits.

These findings and time-delayed bedding plane failures modelled in the previous section are apparently consistent with observations in the field: (1) the aforementioned time-delayed bedding plane failures in highly inclined wells, (2) splintery cavings were observed from breakouts in the thick shale section in the existing vertical well (Fig. 9); such splintery cavings are produced in zones where tensile failures occur throughout the wellbore circumference (Skea et al. 2018). These apparent consistencies suggest the importance of accounting for

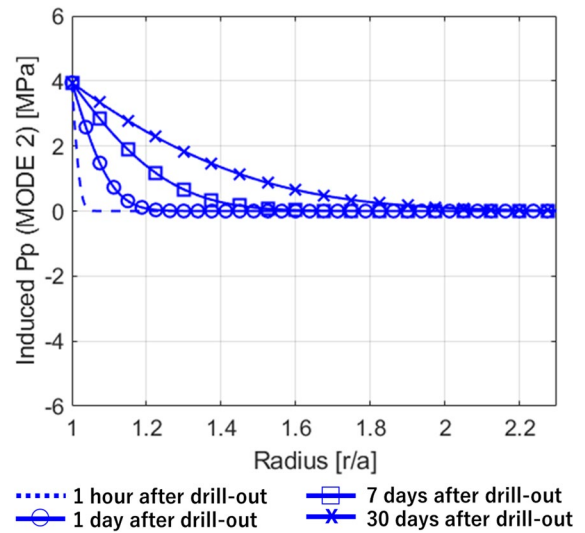


**Fig. 10** Mode 2 induced pore pressure variation with radius

hydraulic-mechanical process to correctly predict the risk of wellbore failure.

Note that utilizing water-based mud would make the time-delayed bedding plane failures even worse because of fluid pressure invasion into the formation. This can easily be simulated by including the mode 2 induced pore pressure and stresses. Mode 2 is axisymmetric and it does not depend on the angular borehole position. Since mud weight is larger than the virgin pore pressure in this example, which is usually the case, mode 2 induced pore pressure shows gradual increase as a function of time (Fig. 10). This pore pressure increase further reduces the normal effective stress acting on bedding plane, which can trigger significant time-delayed bedding plane failures. The maximum/minimum mud weights with the consideration of the mode 2 at 1, 6, 12 h after drill-out are shown in Fig. 11. The minimum mud weight required to prevent bedding plane failure increases as time progresses and becomes larger than the minimum horizontal stress for some highly inclined wells (mud weight limits are closed).

As mentioned earlier, plasticity was not accounted for in the current analysis. Plasticity improves borehole stability significantly and neglecting it may result in suboptimal mud weight limits. Wellbore stability analysis using non-linear stress-strain relation is a solution to this problem, however, it requires many sets of triaxial data. A practical approach would

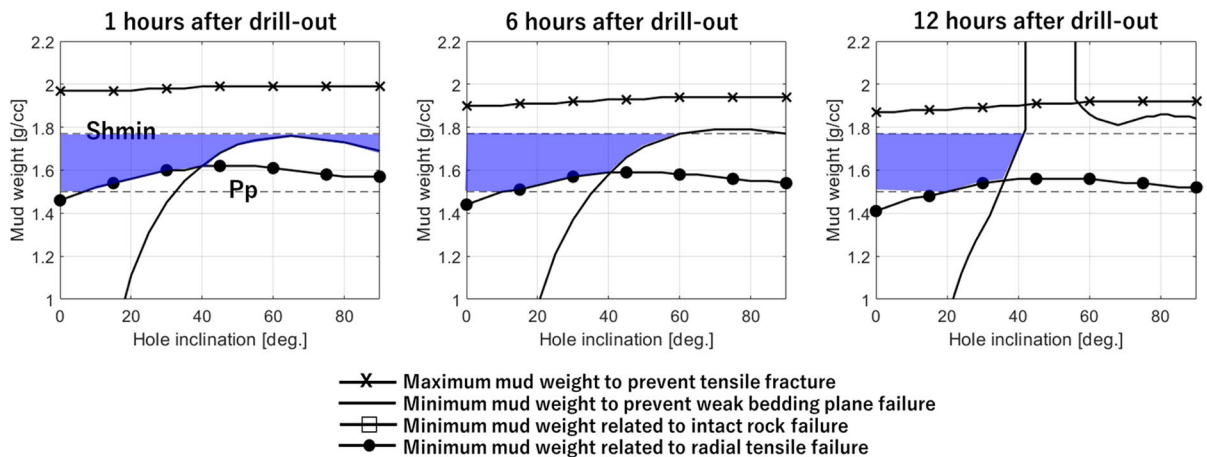


**Fig. 11** Maximum/minimum mud weights for wells drilled subparallel to the maximum horizontal stress direction ( $N70^{\circ}E$ ) based on the stress state at 1, 6, 12 h after drill-out. Mode 2 induced pore pressure and stresses were taken into consideration

therefore be to use adjusted UCS as suggested by Morita and Nagano (2016). It should also be mentioned that plastic deformation would have an impact on the pore pressure evolution as indicated by Duda et al. (2021); Skempton's parameter changes with dilatancy/contractancy of the material. Skempton's parameter based on elasticity, described in this paper, is therefore not valid close to failure. This issue demands further studies.

Last, it should be mentioned that shales are usually anisotropic as underpinned by existing laboratory measurements (e.g. Vernik and Nur 1992; Wang 2002; Szczyk et al. 2018; Lozovyi and Bauer 2019). Shales can be approximated to good accuracy as transversely isotropic and corresponding anisotropic poroelastic model should be utilized to predict wellbore failures precisely. To our knowledge, analytical solutions accounting for hydraulic-mechanical processes are available only for the transversely isotropic material with the plane of isotropy perpendicular to the borehole axis (e.g. Abousleiman and Cui 1998). However, the instantaneous response can be calculated analytically for any material orientations from stress concentration given by the Amadei solution (Amadei 1983; Lekhnitskii 1963) and anisotropic Skempton  $B$  parameters.<sup>1</sup> A comparison

<sup>1</sup> The anisotropic  $B$  for the transversely isotropic material has two invariant components  $B_V$  and  $B_H$ . When translated into common terminology, these can be transformed into the conventional Skempton's  $B$  and  $A$ , where the latter depends on orientation.

of the instantaneous response based on the isotropic approach (the Kirsch solution + isotropic Skempton  $B$ ) has been made with that based on the anisotropic approach using realistic anisotropy parameters. The comparison shows that the difference from the isotropic elastic case can be significant for highly inclined wells drilled in the minimum horizontal stress direction. This is mainly because of anisotropy in Skempton  $B$  (see Asaka and Holt (2021) for detailed comparisons of the instantaneous response). Anisotropic permeability has also been reported (e.g., Mokhtari and Tutuncu 2015; Metwally and Sondergeld 2011). Its impact can be assessed by replacing the permeability coefficient in the poroelastic model with the equivalent permeability coefficient as demonstrated by Ding et al. (2019). They showed that the equivalent permeability coefficient can vary significantly around highly inclined boreholes when the bedding planes are horizontal, and it has certain impact on failure regions and mud weight limits.

## 5 Conclusions

Time-delayed wellbore failures associated with pore pressure diffusion were investigated using the poroelastic model. To account for weak bedding planes, two Mohr–Coulomb failure criteria were adopted. Wellbore stability analysis targeting a particular field with strike-slip stress regime suggested

the importance of accounting for coupled hydraulic-mechanical processes. First, the poroelastic model gives significant time-dependent bedding plane failures for the highly inclined wells subparallel to the maximum horizontal stress direction, which could explain observed wellbore failure. This is because of reduction in normal effective stress acting on bedding plane associated with pore pressure change. Second, the elastic nonporous approach does not give proper mud weight limits to avoid bedding plane failures, especially when there is a fluid pressure invasion into the formation. On the other hand, the poroelastic model gives the maximum mud weight to prevent tensile fractures larger than the elastic nonporous approach. Last, failure regions and modes predicted by the poroelastic model are different from those based on the elastic nonporous approach. For example, radial tensile failures caused by pore pressure increase, which are apparently consistent with the field observation, are not predicted by the elastic nonporous approach. The observations demonstrate that unexpected wellbore failure may happen without consideration of coupled hydraulic-mechanical processes.

**Acknowledgements** We would like to thank INPEX management and all joint venture participants for allowing us to publish this work. This work was supported by INPEX Corporation.

**Disclaimer** The discussions and interpretations mentioned in this paper are purely based on the author's discretion.

**Funding** Open access funding provided by NTNU Norwegian University of Science and Technology (incl St. Olavs Hospital - Trondheim University Hospital). This work was sponsored by INPEX Corporation.

**Availability of data and material** All figures can be reproduced by using parameters listed in Table 1 and equations shown in this paper.

**Code availability** Matlab codes used in this study are available from authors.

**Ethics approval and consent to participate** Not applicable.

**Consent for publication** Not applicable.

**Competing interests** The authors declare that they have no competing interests.

**Open Access** This article is licensed under a Creative Commons Attribution 4.0 International License, which permits use, sharing, adaptation, distribution and reproduction in any medium or format, as long as you give appropriate credit to the original author(s) and the source, provide a link to the Creative Commons licence, and indicate if changes were made. The images or other third party material in this article are included in the article's Creative Commons licence, unless indicated otherwise in a credit line to the material. If material is not included in the article's Creative Commons licence and your intended use is not permitted by statutory regulation or exceeds the permitted use, you will need to obtain permission directly from the copyright holder. To view a copy of this licence, visit <http://creativecommons.org/licenses/by/4.0/>.

## Appendix A: Analytical solutions for the poroelastic problem

According to the loading decomposition scheme proposed by Abousleiman and Cui (1998), the poroelastic problem can be decomposed into three subproblems to simplify the analysis (see also Gao et al. 2017a,b); (I) a poroelastic plane strain problem, (II) an elastic uniaxial stress problem, and (III) an elastic anti-plane shear problem. The principle of superposition is then used to obtain the complete solutions.

### Problem I: Poroelastic plane strain problem

This problem can further be decomposed into three fundamental modes; (1) differential pressure between the far-field isotropic stress and well pressure; (2) differential pressure between virgin pore pressure and well pressure; and (3) a far-field deviatoric stress. Mode 1 and 2 are axisymmetric, which give a homogeneous diffusion equation, while mode 3 is asymmetric. Mode 1 is purely elastic and solutions for radial and tangential stresses are obtained as:

$$\sigma_{rr}^{(1)} = -(\sigma_m - q) \frac{a^2}{r^2}$$

$$\sigma_{\theta\theta}^{(1)} = (\sigma_m - q) \frac{a^2}{r^2} \quad (7)$$

where  $a$  is borehole radius and  $r$  and  $\theta$  are the polar coordinates.

For Mode 2, analytical solutions for induced pore pressure, radial stress and tangential stress can be given in the Laplace transform domain as follows:

$$\begin{aligned} \tilde{p}^{(2)} &= -\frac{p_0 - q}{s} \frac{K_0(\xi)}{K_0(\beta)} \\ \tilde{\sigma}_{rr}^{(2)} &= \frac{2\eta(p_0 - q)}{s} \left[ \frac{a}{r} \frac{K_1(\xi)}{\beta K_0(\beta)} - \frac{a^2}{r^2} \frac{K_1(\beta)}{\beta K_0(\beta)} \right] \\ \tilde{\sigma}_{\theta\theta}^{(2)} &= -\frac{2\eta(p_0 - q)}{s} \left[ \frac{a}{r} \frac{K_1(\xi)}{\beta K_0(\beta)} - \frac{a^2}{r^2} \frac{K_1(\beta)}{\beta K_0(\beta)} + \frac{K_0(\xi)}{K_0(\beta)} \right] \end{aligned} \tag{8}$$

where  $\sim$  denotes the Laplace transform and  $s$  is the Laplace transform variable.  $p_0$  is the virgin pore pressure.  $K_n$  denotes the modified Bessel function of the second kind of order  $n$ ,  $\xi = r\sqrt{s/c}$  and  $\beta = a\sqrt{s/c}$ .  $\eta$  is a function of Skempton  $B$  and drained/undrained rock Poisson's ratio:

$$\eta = \frac{3(\nu_u - \nu)}{2B(1 - \nu)(1 + \nu_u)} \tag{9}$$

Note that, due to the use of synthetic oil which generally prevents fluid pressure invasion into the formation, induced pore pressure and stresses associated with the Mode 2 was set to zero in this case.

For Mode 3, analytical solutions can be given in the Laplace transform domain as follows:

$$\begin{aligned} \tilde{p}^{(3)} &= \frac{\sigma_d}{s} \left[ \frac{B^2(1 - \nu)(1 + \nu_u)^2}{9(1 - \nu_u)(\nu_u - \nu)} C_1 K_2(\xi) \right. \\ &\quad \left. + \frac{B(1 + \nu_u)}{3(1 - \nu_u)} C_2 \frac{a^2}{r^2} \right] \cos 2(\theta - \theta_r) \end{aligned}$$

---


$$\tilde{\sigma}_{rr}^{(3)} = -\frac{\sigma_d}{s} \left[ \frac{B(1 + \nu_u)}{3(1 - \nu_u)} C_1 \left\{ \frac{1}{\xi} K_1(\xi) + \frac{6}{\xi^2} K_2(\xi) \right\} - \frac{1}{1 - \nu_u} C_2 \frac{a^2}{r^2} - 3C_3 \frac{a^4}{r^4} \right] \cos 2(\theta - \theta_r)$$


---

$$\tilde{\sigma}_{\theta\theta}^{(3)} = -\frac{\sigma_d}{s} \left[ -\frac{B(1 + \nu_u)}{3(1 - \nu_u)} C_1 \left\{ \frac{1}{\xi} K_1(\xi) + \left(1 + \frac{6}{\xi^2}\right) K_2(\xi) \right\} + 3C_3 \frac{a^4}{r^4} \right] \cos 2(\theta - \theta_r)$$


---

$$\tilde{\tau}_{r\theta}^{(3)} = -\frac{\sigma_d}{s} \left[ \frac{2B(1 + \nu_u)}{3(1 - \nu_u)} C_1 \left\{ \frac{1}{\xi} K_1(\xi) + \frac{3}{\xi^2} K_2(\xi) \right\} - \frac{1}{2(1 - \nu_u)} C_2 \frac{a^2}{r^2} - 3C_3 \frac{a^4}{r^4} \right] \sin 2(\theta - \theta_r) \tag{10}$$


---

Three constants,  $C_1$ ,  $C_2$  and  $C_3$ , are obtained from the boundary condition at the borehole wall:

$$\begin{aligned} C_1 &= -\frac{12\beta(1 - \nu)(\nu_u - \nu)}{B(1 + \nu_u)(D_2 - D_1)} \\ C_2 &= \frac{4(1 - \nu)D_2}{D_2 - D_1} \\ C_3 &= -\frac{\beta(D_2 + D_1) + 8(\nu_u - \nu)K_2(\beta)}{\beta(D_2 - D_1)} \end{aligned} \tag{11}$$

where

$$\begin{aligned} D_1 &= 2(\nu_u - \nu)K_1(\beta) \\ D_2 &= \beta(1 - \nu)K_2(\beta) \end{aligned} \tag{12}$$

The numerical results in the time domain were obtained by using the inversion technique proposed by Stehfest (1970). These have to be added to the in situ stress components to obtain the complete solution for problem I:

$$\sigma_{rr}^{(I)} = \sigma_{rr}^{(1)} + \sigma_{rr}^{(2)} + \sigma_{rr}^{(3)} + \sigma_m - \sigma_d \cos 2(\theta - \theta_r)$$

$$\sigma_{\theta\theta}^{(I)} = \sigma_{\theta\theta}^{(1)} + \sigma_{\theta\theta}^{(2)} + \sigma_{\theta\theta}^{(3)} + \sigma_m + \sigma_d \cos 2(\theta - \theta_r)$$

$$\tau_{r\theta}^{(I)} = \tau_{r\theta}^{(3)} + \sigma_d \sin 2(\theta - \theta_r)$$

$$\tau_{rz}^{(I)} = \tau_{\theta z}^{(I)} = 0$$

$$p^{(I)} = p^{(2)} + p^{(3)} + p_0 \tag{13}$$

It was found that the results have to be shifted 90 degrees around borehole if  $\sigma_{x,0} \geq \sigma_{y,0}$ . This is probably because the analytical solutions are derived on the condition that  $\sigma_{x,0} < \sigma_{y,0}$  in Detournay and Cheng (1988).

Axial stress can be calculated based on the plane strain assumption:

$$\sigma_{zz}^{(I)} = \nu(\sigma_{rr}^{(I)} + \sigma_{\theta\theta}^{(I)}) + (1 - 2\nu)\alpha p^{(I)} \tag{14}$$

where  $\alpha$  is Biot’s coefficient which can be calculated from Skempton  $B$  and Poisson ratios:

$$\alpha = \frac{3(\nu_u - \nu)}{B(1 - 2\nu)(1 + \nu_u)} \tag{15}$$

**Problem II: Elastic uniaxial stress problem**

This problem is purely elastic for isotropy and its solutions are as follows:

$$\begin{aligned} \sigma_{zz}^{(II)} &= \sigma_{z,0} - \nu(\sigma_{x,0} + \sigma_{y,0}) - (1 - 2\nu)\alpha p_0 \\ \sigma_{rr}^{(II)} = \sigma_{\theta\theta}^{(II)} = \tau_{r\theta}^{(II)} = \tau_{rz}^{(II)} = \tau_{\theta z}^{(II)} = p^{(II)} &= 0 \end{aligned} \tag{16}$$

**Problem III: Elastic anti-plane shear problem**

For isotropy, the shear deformation is uncoupled with the pore fluid flow since it does not produce volumetric strain. Pore pressure is therefore not induced and the solution is the same as the elastic one (e.g. Bradley 1979):

$$\begin{aligned} \tau_{rz}^{(III)} &= (\tau_{xz,0}\cos\theta + \tau_{yz,0}\sin\theta) \left(1 - \frac{a^2}{r^2}\right) \\ \tau_{\theta z}^{(III)} &= (-\tau_{xz,0}\sin\theta + \tau_{yz,0}\cos\theta) \left(1 + \frac{a^2}{r^2}\right) \\ \sigma_{rr}^{(III)} = \sigma_{\theta\theta}^{(III)} = \sigma_{zz}^{(III)} = \tau_{r\theta}^{(III)} = p^{(III)} &= 0 \end{aligned} \tag{17}$$

**Complete solutions**

The complete solution of inclined borehole in isotropic poroelastic medium is obtained by superposition of solutions for problems I-III.

Note that the generalized plane strain assumption adopted here is frequently used in wellbore stability analysis and is valid when the target cross section is far enough from the ends of the borehole (Amadei 1983). Cui et al. (1997b) showed a very good matching between an existing analytical solution using the generalized plane strain assumption (Cui et al. 1997a; essentially the same analytical solution as the one used here), the generalized plane strain finite element, and the three-dimensional finite element solutions.

**References**

Abousleiman Y, Cui L (1998) Poroelastic solutions in transversely isotropic media for wellbore and cylinder. *Int J Solids Struct* 35:4905–4929

Abousleiman Y, Ekbote S (2005) Solutions for the inclined borehole in a porothermoelastic transversely isotropic medium. *J Appl Mech* 72:102–114

Amadei B (1983) *Rock anisotropy and the theory of stress measurements*. Springer, Berlin

Asaka M, Holt RM (2021) Anisotropic wellbore stability analysis: Impact on failure prediction. *Rock Mech Rock Eng* 54:583–605

Asaka M, Sekine T, Furuya K (2016) Geologic cause of seismic anisotropy: a case study from offshore Western Australia. *Lead Edge* 35:662–668

Batzle M, Wang Z (1992) Seismic properties of pore fluids. *Geophysics* 57:1396–1408

Berti M, Simoni A (2010) Field evidence of pore pressure diffusion in clayey soils prone to landsliding. *J Geophys Res* 115:F03031

Biot MA (1941) General theory of three-dimensional consolidation. *J Appl Phys* 12:155–164

Bouteca M, Gueguen Y (1999) Mechanical properties of rocks: Pore pressure and scale effects. *Oil Gas Sci Technol* 54:703–714

Bradley WB (1979) Failure of inclined borehole. *J Energy Resour Technol Trans AIME* 102:232–239

Brewster AC (2015) Using coefficient of consolidation to assess response time and reading accuracy of piezometers in grouted boreholes in fat clays (Masters thesis). The University of Texas at Austin

Castagna JP, Batzle ML, Kan TK (1993) Rock physics—the link between rock properties and AVO response. In: *Offset-dependent reflectivity—theory and practice of AVO analysis*. Investigations in Geophysics, No.8, Society of Exploration Geophysicists, Tulsa, Oklahoma, pp 135–171

- Cornet F, Fairhurst C (1974) Influence of pore pressure on the deformation behavior of saturated rocks. Proceedings of 3rd Congr. ISRM, Denver
- Cui L, Cheng AH-D, Abousleiman Y (1997a) Poroelastic solution for an inclined borehole. *J Appl Mech ASME* 64:32–38
- Cui L, Kaliakin VN, Abousleiman Y, Cheng AH-D (1997b) Finite element formulation and application of poroelastic generalized plane strain problems. *Int J Rock Mech Min Sci* 34:953–962
- Cui L, Abousleiman Y, Cheng AH-D, Roegiers J-C (1999) Time-dependent failure analysis of inclined boreholes in fluid-saturated formations. *J Energy Res Technol* 121:31–39
- Detournay E, Cheng AH-D (1988) Poroelastic responses of a borehole in a non-hydrostatic stress field. *Int J Rock Mech Min Sci Geomech Abst* 25:171–182
- Ding L, Wang Z, Liu B, Lv J, Wang Y (2019) Borehole stability analysis: A new model considering the effects of anisotropic permeability in bedding formation based on poroelastic theory. *J Nat Gas Sci Eng* 69:102932
- Duda MI, Holt RM, Stenebraten JF, Stroisz AM (2021) Effects of plastic deformation on poroelastic pore pressure coefficients in Pierre II shale. 56th U.S. Rock Mechanics/Geomechanics Symposium
- Fjaer E, Holt RM, Horsrud P, Raaen AM, Risnes R (2008) *Petroleum related rock mechanics*, 2nd edn. Elsevier, Amsterdam
- Fossen H (2016) *Structural geology*, 2nd edn. Cambridge University Press, Cambridge
- Gao J, Deng J, Lan K, Song Z, Feng Y, Chang L (2017a) A porothermoelastic solution for the inclined borehole in a transversely isotropic medium subjected to thermal osmosis and thermal filtration effects. *Geothermics* 64:114–134
- Gao J, Deng J, Lan K, Feng Y, Zhang W, Wang H (2017b) Porothermoelastic effect on wellbore stability in transversely isotropic medium subjected to local thermal non-equilibrium. *Int J Rock Mech Min Sci* 96:66–84
- Ghassemi A, Diek A (2002) Porothermoelasticity for swelling shales. *J Petrol Sci Eng* 34:123–135
- Hachem HA (2017) Modeling of pore pressure propagation and dissipation in compressible porous media (Masters thesis). The University of Texas at Austin
- Hiramatsu Y, Oka Y (1962) Analysis of stress around a circular shaft or drift excavated in ground in a three dimensional stress state. *J Min Metall Inst Jpn* 78:93–98
- Holt RM, Bauer A, Bakk A (2018b) Stress-path-dependent velocities in shales: impact of 4D seismic interpretation. *Geophysics* 83:MR353–MR367
- Holt RM, Bakk A, Bauer A (2018a) Anisotropic poroelasticity—does it apply to shale? 88th Annual International Meeting, SEG, Expanded Abstracts, 3512–3516.
- Horsrud P, Bostrom B, Sønstebo EF, Holt RM (1998) Interaction between shale and water-based drilling fluids: laboratory exposure tests give new insight into mechanisms and field consequences of KCl contents. SEP 48986. In: SPE Annual Technical Conference and Exhibition, New Orleans, Louisiana, 27–30 September
- Iverson RM (2000) Landslide triggering by rain infiltration. *Water Resour Res* 36:1897–1910
- Jaeger JC, Cook NGW (1979) *Fundamental of rock mechanics*, 3rd edn. Chapman and Hall, London
- Kanfar MF, Chen Z, Rahman SS (2015) Effect of material anisotropy on time-dependent wellbore stability. *Int J Rock Mech Min Sci* 78:36–45
- Kirsch EG (1898) Die Theorie der Elastizität und die Bedürfnisse der Festigkeitslehre. *Zeitschrift Des Vereines Deutscher Ingenieure* 42:797–807
- Lee H, Ong SH, Azeemuddin M, Goodman H (2012) A wellbore stability model for formations with anisotropic rock strengths. *J Petrol Sci Eng* 96:109–119
- Lekhnitskii SG (1963) *Theory of the elasticity of anisotropic bodies*. Holden-Day, San Francisco
- Lozovyi S, Bauer A (2019) Static and dynamic stiffness measurements with Opalinus Clay. *Geophys Prospect* 67:997–1019
- Ma T, Chen Y, Duan M (2018) Chemo-poroelastic coupling method for wellbore stability analysis in shale gas formation with weakness planes. *Geotech Geol Eng* 36:1817–1831
- MacBeth C, HajNasser Y, Stephen K, Gardiner A (2011) Exploring the effect of meso-scale shale beds on a reservoir's overall stress sensitivity to seismic waves. *Geophys Prospect* 59:90–110
- Metwally YM, Sondergeld CH (2011) Measuring low permeabilities of gas-sands and shales using a pressure transmission technique. *Int J Rock Mech Min Sci* 48:1135–1144
- Mody FK, Hale AH (1993) Borehole stability model to couple the mechanics and chemistry of drilling fluid shale interaction. *J Pet Technol* 45:1093–1101
- Mokhtari M, Tutuncu AN (2015) Characterization of anisotropy in the permeability of organic-rich shales. *J Pet Sci Eng* 133:496–506
- Morita N, Nagano Y (2016) Comparative analysis of various failure theories for borehole breakout predictions. SPE Annual Technical Conference and Exhibition
- Rice JR, Cleary MP (1976) Some basis stress diffusion solutions for fluid-saturated elastic porous media with compressible constituents. *Rev Geophys Space Phys* 14:227–241
- Roohi A (2017) Mathematical approach of MSE in thermo-poro-elastic conditions improves decision making to use bore hole enlargement (BHE) (PhD Dissertation). University of Leoben
- Skea C, Rezagholilou A, Far PB, Gholami R, Sarmadivleh M (2018) An approach for wellbore failure analysis using rock cavings and image processing. *J Rock Mech Geotech Eng* 10:865–878
- Smith TM, Sondergeld CH, Rai CS (2003) Gassmann fluid substitutions: a tutorial. *Geophysics* 68:430–440
- Stehfest H (1970) Numerical inversion of Laplace transforms. *Commun Ass Comput Mach* 13:47–49
- Szewczyk D, Bauer A, Holt RM (2018) Stress-dependent elastic properties of shales-laboratory experiments at seismic and ultrasonic frequencies. *Geophys J Int* 212:189–210

- Vernik L, Nur A (1992) Ultrasonic velocity and anisotropy of hydrocarbon source rocks. *Geophysics* 57:727–735
- Wang Z (2002) Seismic anisotropy in sedimentary rocks, part 2: laboratory data. *Geophysics* 67:1423–1440

**Publisher's Note** Springer Nature remains neutral with regard to jurisdictional claims in published maps and institutional affiliations.